Article

Flood Risk Assessment Index for Urban Mobility with the Aid of Quasi-2d Flood Model Applied to an Industrial Park in São Paulo, Brazil

Matheus Martins de Sousa [1,*], Osvaldo Moura Rezende [1], Ana Caroline Pitzer Jacob [2], Luiza Batista de França Ribeiro [2], Paula Morais Canedo de Magalhães [3], Gladys Maquera [4] and Marcelo Gomes Miguez [1,3]

[1] Escola Politécnica, Universidade Federal do Rio de Janeiro (UFRJ), Rio de Janeiro 21941-909, Brazil
[2] Aquafluxus Water Resources Environmental Consulting, Rio de Janeiro 21941-972, Brazil
[3] Programa de Engenharia Civil—COPPE, Universidade Federal do Rio de Janeiro, Rio de Janeiro 21941-909, Brazil
[4] Grupo de Investigación INARI, Universidad Peruana Unión, Lima 15464, Peru
[*] Correspondence: matheus@poil.ufrj.br; Tel.: +55-21-3938-7830

Abstract: Risk can be defined as the relationship between the likelihood of a hazard causing a potential disaster and its consequences. This study aims to assess the likelihood that a new industrial region, located in the state of São Paulo (Brazil), will be flooded, causing the disruption of the mobility system and local economic activities. To fulfill this aim, a new approach is proposed by combining the vector information of the highway network that serves the region with the result of a quasi 2-D raster flood model, generating a set of interpreting rules for classifying the safety of routes. The model called MODCEL is a quasi-2D hydrodynamic model that represents the watershed using compartments called cells, and it was adapted to work using a raster file format in which each pixel is represented as a flow cell connected to its surroundings by the Saint-Venant equations without the inertia terms. Therefore, this study proposes an assessment framework that can be replicated for similar problems of flood risks to mobility. The possible effects of flood events on the accessibility to areas of interest are determined, indicating a possible disruption to economic activities and transportation and allowing for planning alternatives in advance.

Keywords: floods; urban mobility disruption; transport flood risk assessment; quasi-2D raster modeling

1. Introduction

There is a strong correlation between urban development, flooding, and flood protection measures. Protection works have been triggered by development, but also development has been boosted by the existence of protection works [1]. This means that the sense of safety introduced by flood defense works tends to favor urban development in originally hazardous areas.

This may be a controversial trend, as it can increase the residual risks as a consequence. Therefore, flood risks may increase, in fact, even in "protected areas", since the exposure of goods and people can be intensified by the false perception of complete safeness [2]. That is, the territory put in safe conditions by hydraulic works is only safe under a certain threshold, since every project is defined for a certain reference event related to a determined return period.

In fact, this trend can be seen in many countries, where a large number of cities have been built or developed in disaster-prone regions [3]. Hence, recognizing the range of possible threatening impacts of floods is important for successfully establishing an effective flood risk management process [4].

It is noteworthy that flooding may cause serious problems in the cities' infrastructure systems and, as a consequence, affect essential products and service provisions. In the state

of São Paulo, where the largest Brazilian industrial park is located, many companies suffer serious financial and competitiveness losses due to excessive rainfall and floods. According to the Research Department of the Industrial Federation of São Paulo State (FIESP) [5], 59% of the state industries are negatively affected by flooding, which result in delays in the supply chain, due to failure in the transportation service, increasing the information demand for planning and studies to mitigate losses.

Therefore, the contribution of this study lays on a proposal of a flood risk assessment framework, based on hydrodynamic modeling, that aims to evaluate the potential damage in the mobility system of a new industrial park located in the state of São Paulo (Brazil). To fulfill this aim, a new approach is proposed by combining the vector information of the highway network that serves the region with the result of a quasi 2-D raster flood model, generating a set of interpreting rules for classifying the safety of routes.

This work will help decision-makers assess the practicability of creating alternative routes, or to increase its flood defense, to find an optimal strategy that significantly reduces flood-induced delays.

The proposed framework, presented in more detail in the next section, was applied to a case study, but it can be replicated for similar problems of flood risks to mobility in any other region.

2. Literature Review

2.1. Risk Assessment Definitions

Risk, hazard, and related definitions are found in several documents, such as [6,7]. For the United Nations [8], risk is constituted by the probability of having negative consequences or expected losses (to the individual property, goods, interruption of economic activities, and environmental damage), resulting from interactions between natural or man-induced hazards and the conditions of the vulnerability/capacity of the system.

Hazard, instead, refers to "a dangerous phenomenon, substance, human activity or condition that may cause loss of life, injury or other health impacts, property damage, loss of livelihoods and services, social and economic disruption, or environmental damage" [8]. Natural hazards usually cannot be controlled or reduced. The risk, in turn, is liable to be managed by minimizing its impacts on the interest system [9].

Vulnerability can be understood, in a general way, as the degree to which a system is likely to experience harm, due to exposure to a hazard [10]. At last, resilience refers to the way in which the population and organizations manage to respond positively to the adverse conditions of an event [11].

In urban flood studies, hazard is triggered by the occurrence of intense rainfalls that interact with the watershed to produce discharges and, eventually, flooding. Then, it will be a function of the probability of flood occurrence, while its consequences will depend on the flood properties, such as flood depths, duration, and flow velocity. On the other side, local vulnerability will define how critical these flood properties are, depending on physical, social, economic, and environmental factors, which can intensify the susceptibility of a given community to the impacts of a given hazard [12].

2.2. Urban Transport Disruption

Critical infrastructures provide essential products and services to cities, including transportation, drinking water, water treatment, energy, telecommunications, information technology, food, banking and finance, public health and healthcare, commercial facilities, and emergency services [13–15].

It is noteworthy that these infrastructure systems, in modern cities, are connected directly or indirectly through one or more intervening components. Therefore, disruption or failure of one component can propagate through the network and subsequently affect the other components [14,15].

In this sense, disruptions to such systems can cause drastic socioeconomic consequences and impede the development of sustainable cities [16]. Therefore, reliable and

secure operations of infrastructure systems are indispensable to national well-being and development [15].

In this sense, extensive research has been conducted to evaluate the impacts of flooding on communities and economies [17]. However, fewer studies have been focused on the vulnerability of the infrastructure system to flooding events and the consequences on the corresponding services [15,18,19].

Regarding the weather-related disruption of the transport sector, flooding is considered its prevalent cause [20,21]. When flooding closes a certain road, not only are the cars directly caught by water affected, but a greater part of the transportation network may be affected by the consequent traffic jam. As the transportation network enables the movement of people and goods and is the basis of economic activities, its disruption may have drastic socio-economics consequences [16]. According to the World Bank [22], approximately 73% of global expected annual damage (EAD) is caused by surface and river floods. Additionally, the average global EAD for transport infrastructure assets is $14.6 billion and about $8 billion in low and middle-income countries.

The functionality of a transportation network is based on many factors, but, in theory, if vehicles traveling on roads can drive near the roads' speed limit, there would be no notable congestion, except at peak traffic hours. However, in the case of flood events, some roads may have diminished their level of service, resulting in a decreased transportation-network effectiveness [23].

In this sense, some researchers have developed methodologies for flood risk assessment, considering the transport system disruption. It is known that flooding on a road does not necessarily preclude people from driving along it [20]. Therefore, in order to transition from a binary view of a flooded road being considered 'open' or 'closed', a more complete approach considering the relationship between the flood depths and the disruption of the road transport system can be established. Usually, this relationship considers the flood depth and the impact on the vehicle's speed and on the road network connectivity [20,24,25].

In the [20] study, the function that describes the relationship between the depth of standing water and vehicle speed was constructed by fitting a curve to video analysis supplemented by a range of quantitative data that has been extracted from existing studies and other safety literature. The main advantage of this methodology is that it is simple to incorporate this proposed function into existing transport models to produce better estimates of flood induced delays.

Another interesting study was carried out by [15]. The authors proposed a flood risk assessment framework for interdependent infrastructure systems based on the strongest path method (SPM) and 2D hydrodynamic modelling. The model investigates the impacts of direct and indirect connections among infrastructure systems, explores their relative importance in the network, and prioritizes the associated risks for more efficient resource allocation.

In the study carried out by [26] the vulnerability is determined by a susceptible-impacted-susceptible (SIS) diffusion model to capture the impact of flooding on the road network connectivity. With model results, the authors were able to estimate a relationship between vehicle speed and flood depth on road networks.

Some other authors have developed this same relationship vehicle speed and flood depth but using hydrodynamic models. In the [25] study, the authors calculated the flooding level in urban areas, caused by rainfall, by using the spatial runoff assessment tool (S-RAT) and the flood inundation model (FLO-2D model). Using modelling results, they combined a flood–vehicle Speed curve and a rainfall–flood depth curve to prepare a traffic disruption map.

Another similar approach was undertaken by [24], where the flood depth was modeled using a static and hydrodynamic model and then assigned to each road segment. After that, flood depth was turned into one of the factors that causes an increase in travel time.

Also using hydrodynamic modelling, ref. [27] proposed an integrated framework linking meteorological information, land use functions, and hydrodynamic models with a safety speed function to relate flood depth to a reduction in speed in order to determine road network vulnerability.

Considering the consulted references, this study intends to present a flood risk assessment framework that also correlates the flood depths with the disruption of the road transport system. The proposed methodology is based on the combination of vector information of the highway network that serves the region with the result of a quasi 2-D raster flood model, generating a set of interpreting rules for classifying the safety of routes.

3. Materials and Methods

Flood risks to mobility assessment must consider the available routes, land use, occupation patterns, and flood characteristics, establishing reference indicators to assess lock down conditions [28]. In this context, a specific flood risk assessment framework for urban mobility was developed.

The proposed framework (as seen in Figure 1) was elaborated in four stages: (1) the identification of previous studies, (2) the vulnerability to flood assessment, (3) the flood hazard assessment, and (4) the flood risk assessment. More details regarding each phase are presented in the following.
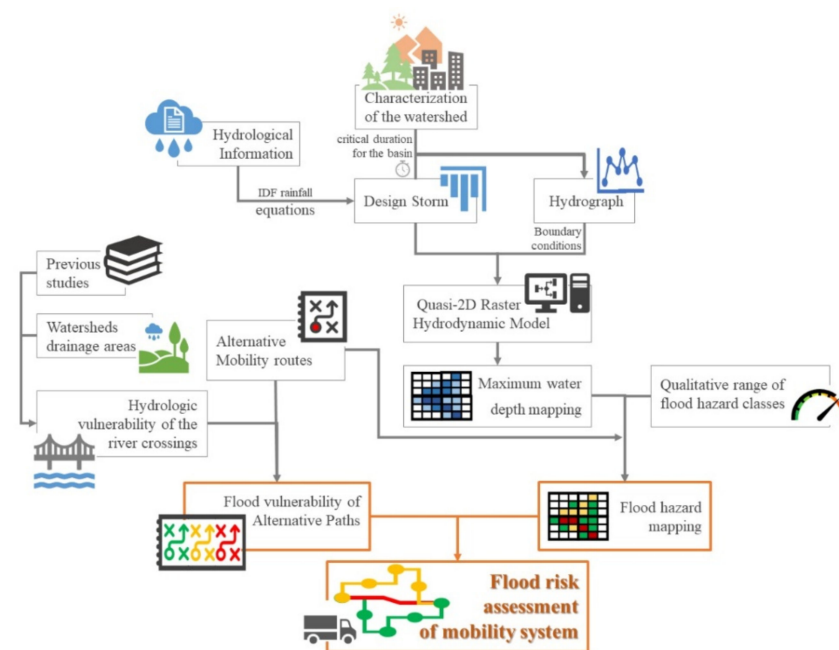

Figure 1. Adopted methodology.

3.1. Study Area

The state of São Paulo, southeast region of Brazil, has a total area of 248,193.1 km^2 (~2.9% of the entire country) and approximately 43.7 million inhabitants (~22% of Brazilian population). Its urbanization level is about 96.37%, which shows its high urban expressiveness [29].

This state also has the highest Brazilian GDP, corresponding to 32.5% of the national GDP. The two most significant economic activities undertaken inside the state are services (77.02% of GDP) and industries (21.43%) [29].

Considering the importance of industries in state economics, this research presents a case study that consists of the evaluation of alternative entry and exit routes of a new industrial park located in the state of São Paulo, as shown in Figure 2.
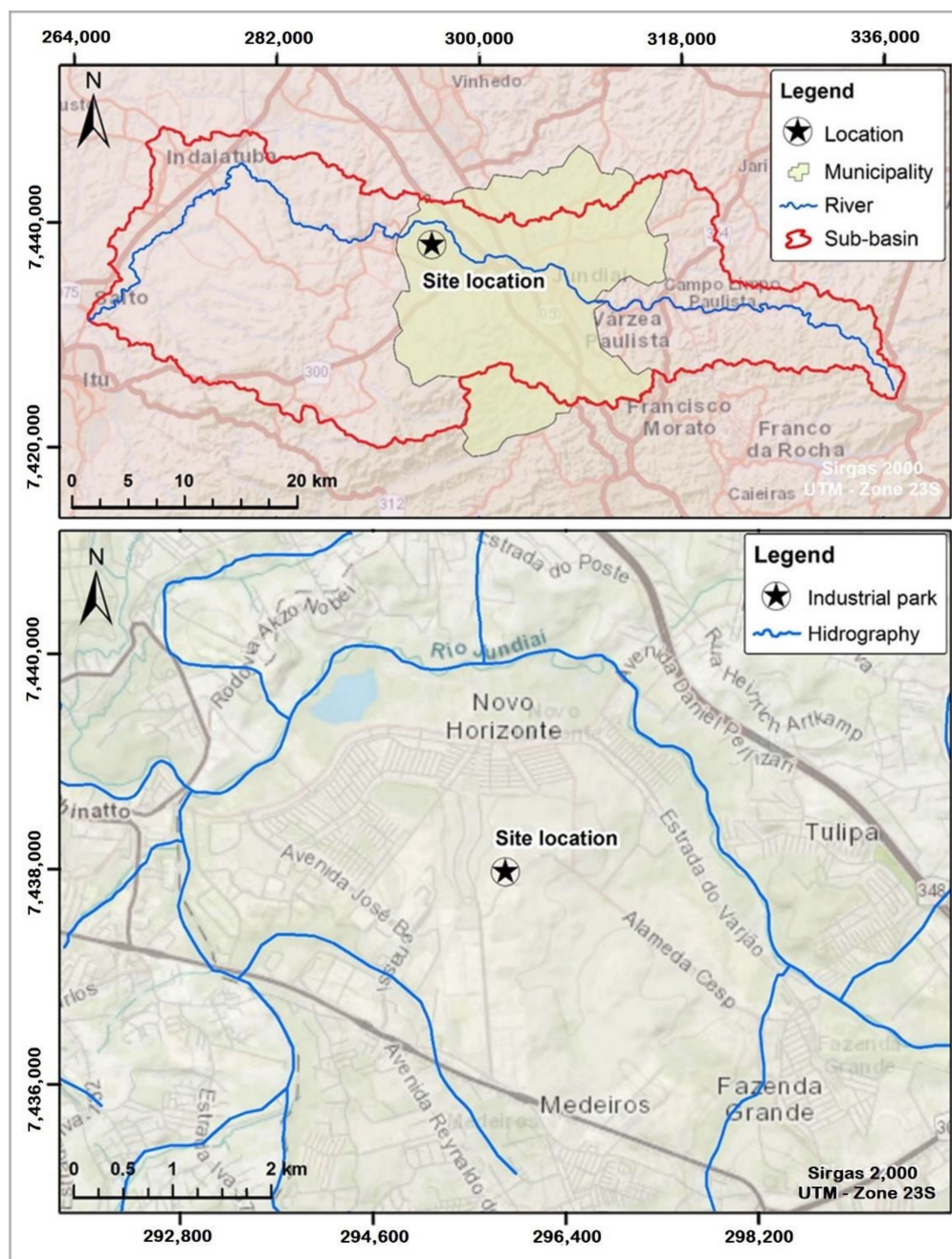
Figure 2. Site location in the watershed–SP and industrial park region, with the main local watercourses and roads. (Data source: [30]).

3.2. Research Procedure

3.2.1. Phase 1: Previous Studies

The first phase of the proposed methodology consisted of raising information of the studies carried out at three levels of government: federal, state, and municipal.

Previous studies were gathered to better understand the region where the interest site is located and to identify the most vulnerable areas to flood events. These studies will help to assess the site's vulnerability to flooding.

3.2.2. Phase 2: The Vulnerability to Floods Assessment

Streets and highways connect regions and contribute to their economic development. Flood events not only injury the traffic but can also damage the structures of bridges and crossings and affect economic activities. This situation particularly affects industrial areas

where interruptions in the pathways can lead these sites to have severe supply chain crises, isolation, and even affect their operations.

In this sense, the vulnerability to the flood indicator should point to how vulnerable to floods the mobility systems and the interest site itself are. In this study, the flood vulnerability assessment follows a general qualitative classification, as shown in Table 1.

Table 1. Qualitative range of flood vulnerabilities classes.

	Flood Vulnerability Classes	Flood Vulnerability Ranges
	very low	0.00–0.15
	low	0.15–0.30
	moderate	0.30–0.50
	high	0.50–0.75
	very high	0.75–1.00

The flood vulnerability assessment was made according to the following steps:

1. Indicating the possible routes between the site and the nearest highway.
2. Highlighting the existing bridges and culverts on each route.
3. Defining the watershed area of each river crossing (bridges and culverts).
4. Calculating the hydrological vulnerability of each river crossing based on the normalization of its watershed area with values between 0 and 1, with a higher value being more vulnerable (Equation (1)).

$$hv = f_{norm}(wa) \qquad (1)$$

where:

wa—watershed areas of each river crossing (m^2);
hv—hydrological vulnerability of a river crossing;
f_{norm}—area normalization function. The area equivalent to the density value for the third quartile of the entire sample is taken as a reference value. Any watershed with an area greater than this reference value is at the maximum normalized value, that is equal to 1. For watersheds with areas smaller than this reference, the normalized value is based on a linear distribution. This procedure was made to reduce possible "flattening" of the evaluation scale, due to the presence of extreme values.

5. Computing the route vulnerability. The route vulnerability is then given by the highest value among two options (OP 1 and OP 2). This configuration aims to eliminate the potential bias of routes with several river crossings, but only a few of them with high vulnerability, in a situation that could lead to a false low value of vulnerability. The adopted options were:

- OP 1: the route vulnerability is given by the simple average of the hydrological vulnerability of all existing river crossings on the route (Equation (2));

$$RV_{OP\,1} = \frac{\sum_{i=0}^{n} hv_i}{n} \qquad (2)$$

where:

$RV_{OP\,1}$—route vulnerability option 1;
hv—hydrological vulnerability of existing river crossings on the route;
n—number of all of the existing river crossings on the route.

- OP 2: the route vulnerability is given by the normalization of the average watershed area of all river crossings on its way. Firstly, the average area of the watershed of all river crossings on each route is taken (Equation (3)). Then

this average area value is normalized with the same normalization function previously presented (Equation (4)).

$$AWA = \frac{\sum_{i=0}^{n} wa_i}{n} \tag{3}$$

$$RV_{OP\ 2} = f_{norm}(AWA) \tag{4}$$

where:

AWA—average of watershed areas of all river crossings on the route (m²);
wa—watershed areas of each river crossing on the route (m²);
n—number of all of the existing river crossings on the route.
$RV_{OP\ 2}$—route vulnerability option 2;

3.2.3. Phase 3: The Flood Hazard Assessment

The flood hazard assessment is based on the maximum water depths resulting from a hydrodynamic simulation of intense rainfall, with 100 and 500 years of return period (H_{100} e H_{500}, respectively), over the watershed. The hazard is then classified in a qualitative range, according to Table 2. This classification is adapted from [20], who proposed a depth break function for road transport.

Table 2. Qualitative range of flood hazard classes.

	Flood Hazard Classes	Flood Depth (cm)
	very low	<20
	low	20–30
	moderate	30–40
	high	40–60
	very high	>60

To map flood depths, hydrologic and hydrodynamic mathematical modeling tools were used, as shown in the following.

Hydrological studies.

The hydrological study aims to elaborate the design rainfall events, related to the chosen return periods, as inputs to the hydrodynamic studies.

The duration of rainfall is inversely proportional to rainfall intensity. Thus, the shorter the rainfall duration, the greater its intensity. Short-term rainfall tends to cause higher runoff peaks in the drainage network, while longer rainfalls result in higher water volumes in the system. To evaluate the worst scenario, a design rainfall was taken with a duration equivalent to the time of concentration of the watershed, highlighting the effect of higher flood peak values.

The necessary hydrological information refers to the historical rainfall series measured in the region, which enables the elaboration of IDF (intensity-duration-frequency) equations to local rainfall. The design rainfall events, with a critical duration for the watershed and related to 100 and 500 years of return period, were elaborated based on these equations.

The resulting hydrographs, obtained by the application of the synthetic unit hydrograph [31], were used as boundary conditions for hydrodynamic modeling.

For the hydrodynamic studies, the modeling tool called MODCEL was used as a flow-cellular model for urban watershed representation. MODCEL is originally a quasi-2D model [32] that represents the urban space using a set of homogeneous compartments, called cells. The concept of flow cells was initially developed by [33] and enshrined by [34].

The cells cover the whole space of the watershed in an interconnected way, forming a flow network, linked by one-dimensional equations. Thus, MODCEL can represent the two-dimensional characteristics of the watershed in a simplified way, only using 1D equations. MODCEL is also integrated with a hydrological module that performs the rainfall-runoff transformation in each cell, using a modified rational method and considering a storage capacity in each cell.

The variation of the water volume in a cell *i*, in a time interval *t*, is given by the mass balance in this cell. Thus, in differential terms, we have the following continuity equation (Equation (5)):

$$A_{s_i} \frac{dZ_i}{dt} = P_i + \sum_k Q_{i,k} \tag{5}$$

where:

$Q_{i,k}$—discharge between neighboring cells *i* and *k*;
Z_i—water level in the center of the cell *i*;
A_{si}—the surface area of the water mirror in the cell *i*;
P_i—discharge produced by the rainfall occurring on the cell *i*;
t—independent time variable.

In the MODCEL, the temporal discretization of the differential equation (Equation (5)) is made by numerically linearizing all nonlinear terms, so that there is no need for an iterative solution procedure in order to simplify the numerical model. The discharges are expanded in the Taylor series. The cell links are defined by the modeler according to the characteristics observed in the topographic and urban fabric analysis of the region to be modelled.

MODCEL is in continuous improvement, and it is used as an alternative for modeling complex urban areas. MODCEL can be found in detail in [35] and some of its applications can be found in [36–40].

In this study, however, MODCEL was used as a raster model to represent the region of interest in an automatic way. Raster models are those that transform each point of a digital elevation model (DEM) or digital terrain model (DTM) in a "pixel". In this case, the structure of MODCEL was adapted so that each pixel represents a flow cell that is connected to the other cells in its surroundings by the Saint-Venant dynamic equation, without the inertia terms, as represented schematically in Figure 3.
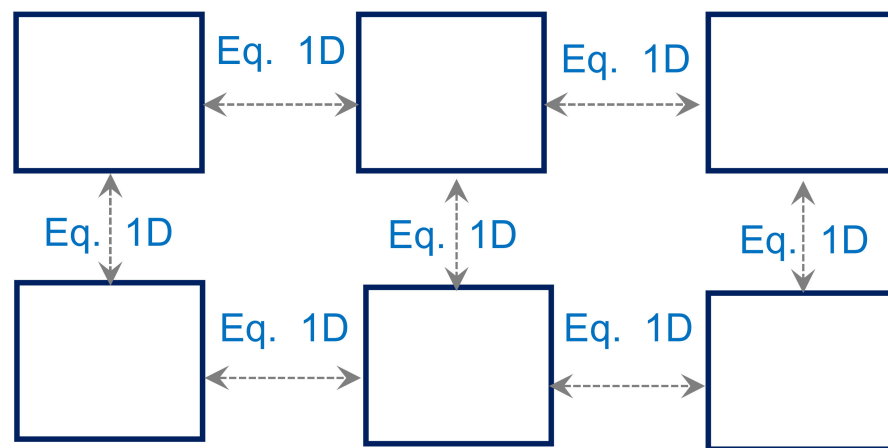

Figure 3. Schematic representation of the connection between MODCEL-raster cells/pixels.

This type of model has increasingly gained credibility for floodplain modeling [41–50]. The main advantage of these models is the processing speed [51]. However, it is necessary to find the equilibrium between the best resolution of the modelled area and the computational cost [52], without disregarding the cost of surveying.

3.2.4. Phase 4: The Risk Assessment

The flood risk assessment indicates how prone to suffering the impacts from floods are on the mobility systems and the site itself, which is estimated through the product between the vulnerability and the hazard. The general equation used to calculate the flood risk is given by Equation (6):

$$R = V^{0.25} \cdot [0.83 \cdot H_{100} + 0.17 \cdot H_{500}]^{0.75} \tag{6}$$

where:

R—flood risk;
V—flood vulnerability;
H_{100}—Flood hazard for the 100-year storm. Equivalent to the maximum flood depth resulting from the 100-year storm;
H_{500}—Flood hazard for the 500-year storm. Equivalent to the maximum flood depth resulting from the 500-year storm.

The choice of a product allows for cancelling the final risk if one of the parcels is equal to zero. Thus, if there is no vulnerability, there is no risk, because there is no exposure, or yet, if there is no hazard, there is no risk, because there is no impact cause.

The weight system applied to the hazard indicators (H_{100} e H_{500}) considered the probability of the occurrence of each event. The flooding event resulting from the 100-year storm has a probability of occurrence equal to 1% in a given year, while one from the 500-year storm has a probability equal to 0.2%. Thereby, the 100-year storm has a chance of occurrence that is five times greater than the 500-year storm. This result was used to define the weight of the indicators, rounded to two decimal places.

The equation is weighted to give more importance to the hazard that characterizes the potential impact of the flooding event. This decision was the result of a modeler decision and can be revised in each particular application.

Finally, the flood risk classification received a qualitative range, as shown in Table 3.

Table 3. Qualitative range of flood risk classes.

	Flood Risk Classes	Flood Risk Ranges
	very low	0.00–0.15
	low	0.15–0.30
	moderate	0.30–0.50
	high	0.50–0.75
	very high	0.75–1.00

The flood risk assessment of a mobility system considers the flood vulnerability of each potential route, accounting for the hazard indicator encountered along the route path.

To make it possible, it detached all flood hazard values from flow cells that are superimposed by route path. Each cell receives a risk value (Equation (6)) considering the flood depths in the cell and the vulnerability of the route. Then, the risk along the route is recalculated by the moving average of three consecutive cells (~180 m). This definition is proposed to guarantee that there is a systematic flooded reach, and not only a small local spot in one cell/pixel. In this way, the maximum risk will be achieved only when the route presents a continuous stretch with at least 180 m (probably more) in length with a maximum flood risk ($R = 1$). This configuration also indirectly measures the recession time of flooding, once long stretches of flooded areas tend to have a slower flood recession.

4. Results

4.1. Phase 1: Previous Studies

The information obtained from previous studies allows an overview about flooding characteristics on the industrial park surrounding areas. Studies were carried out at three levels of government: federal, state, and municipal.

The region of the industrial park site does not show any riverine paths prone to floods, accordingly to ANA (National Water Agency) [53], but a CPRM (Geological Survey of Brazil) study [54] indicates several susceptible areas inside the municipality territory. The municipality administration indicates a large flooding zone, and a part of this flooding zone reaches the industrial park neighborhood.

Figure 4 shows the existing flood risk information at the industrial park region, consolidated in a single map composed of flood vulnerability [54] and susceptibility [53], intending to offer a comparison with the obtained results in the present study. The flooded

area mapped in the drainage management plan of the municipality is also plotted in the same figure.
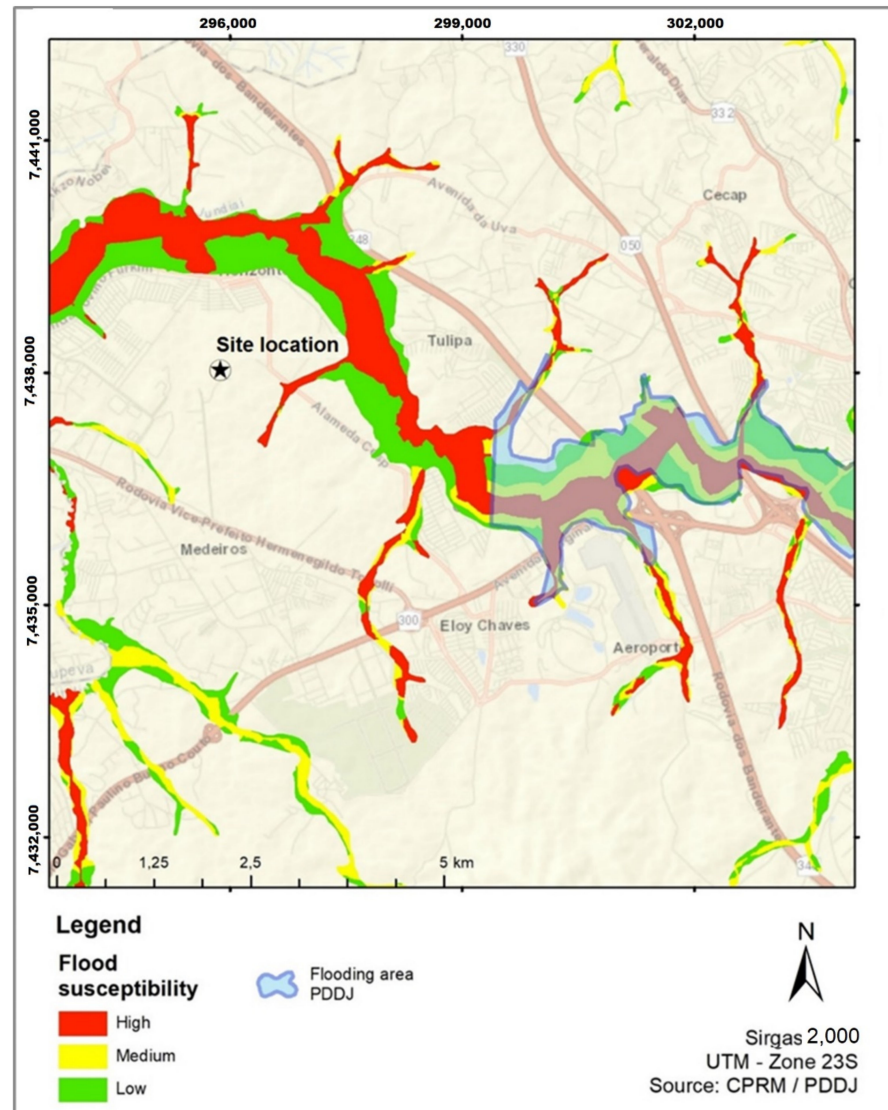

Figure 4. Consolidation of existing flooding maps in the industrial park region.

Generally, from the information found in the existing studies, it is possible to notice that the industrial park is not directly exposed to common flood events. The site is located on a plateau, several meters above the valleys of the neighboring rivers. However, flood events have a high chance of indirectly affecting the site of interest, blocking transportation or disrupting public services.

4.2. Phase 2: The Flood Vulnerability Assessment

The vulnerability assessment of the industrial park aimed to classify its propensity to suffer critical impacts from flood events, which could result in the disruption of mobility systems.

As mentioned before, the flood vulnerability assessment is given by the number of accesses to the site, considering the closer highway, as well as the hydrological vulnerability of the various river crossings existing in the path.

The methodology adopted for the flood vulnerability assessment starts by indicating the possible routes between the site and the nearest highway, and also identifying the existing bridges and culverts on each route.

The main accesses to the industrial park are highways A and B, both located on the west side of the site. The access to these highways can be achieved through four routes: Route 1, Route 2, Route 3, all of them with three river crossings, and Route 4 with six river crossings. Figure 5 shows all four routes and their river crossings, called T2 until T13.
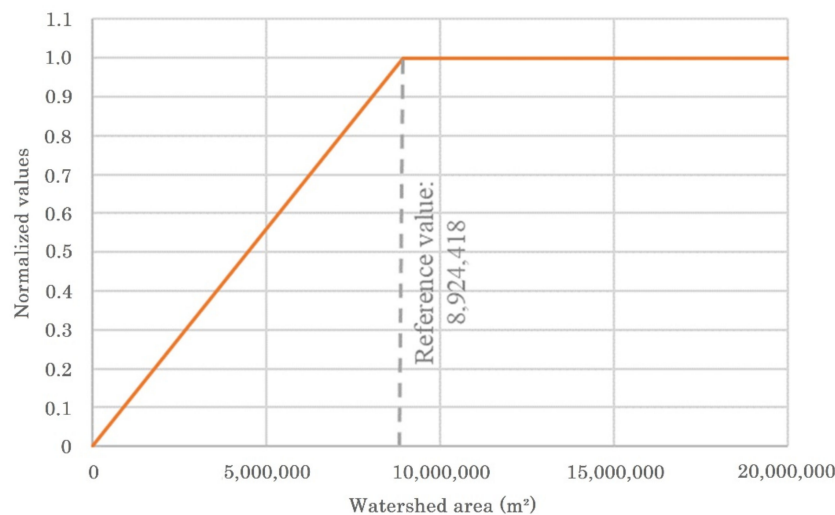

Figure 5. Normalization function used to calculate the hydrological vulnerability and in the normalization of the average area of all river crossings on a route.

In sequence, the watershed area for each river crossing must be determined. Table 4 shows, in its second column, the watershed areas of all river crossings and the refence value up to maximum vulnerability, taken as equal to the third quartile of the watershed area distribution. The function used in the area normalization and to calculate the hydrological vulnerability of river crossings is show in Figure 5.

Table 4. Flood vulnerability evaluation of mobility of industrial park site.

Route	River Crossing	Watershed Area of Each River Crossing	Hydrological Vulnerability	Route Vulnerability OP 1	Average of Watershed Area of All River Crossings on the Route	Route Vulnerability OP 2	Final Route Vulnerability
1	T10	1,305,083	0.15	0.60	79,432,076	1	1
	T11	2,270,885	0.25				
	T12	98,220,736	1.00				
	T13	215,931,600	1.00				
2	T9	459,834	0.05	0.61	5,597,322	0.63	0.63
	T8	6,772,344	0.76				
	T2	5,766,430	0.65				
	T3	9,390,680	1.00				
3	T9	459,834	0.05	0.52	4,788,740	0.54	0.54
	T8	6,772,344	0.76				
	T4	2,532,100	0.28				
	T3	9,390,680	1.00				
4	T9	459,834	0.05	0.56	6,223,719.67	0.70	0.70
	T8	6,772,344	0.76				
	T4	2,532,100	0.28				
	T5	7,525,630	0.84				
	T6	3,680,110	0.41				
	T7	16,372,300	1.00				
Reference Value		8,924,418					

Once calculated and once the hydrological vulnerability of each river crossing is identified, it is possible to calculate the route vulnerability. Its value is given by the highest value among two options (OP 1 and OP 2) previously described.

Finally, Table 4 and Figure 6 also show the vulnerability evaluation of potential routes of the industrial park site.
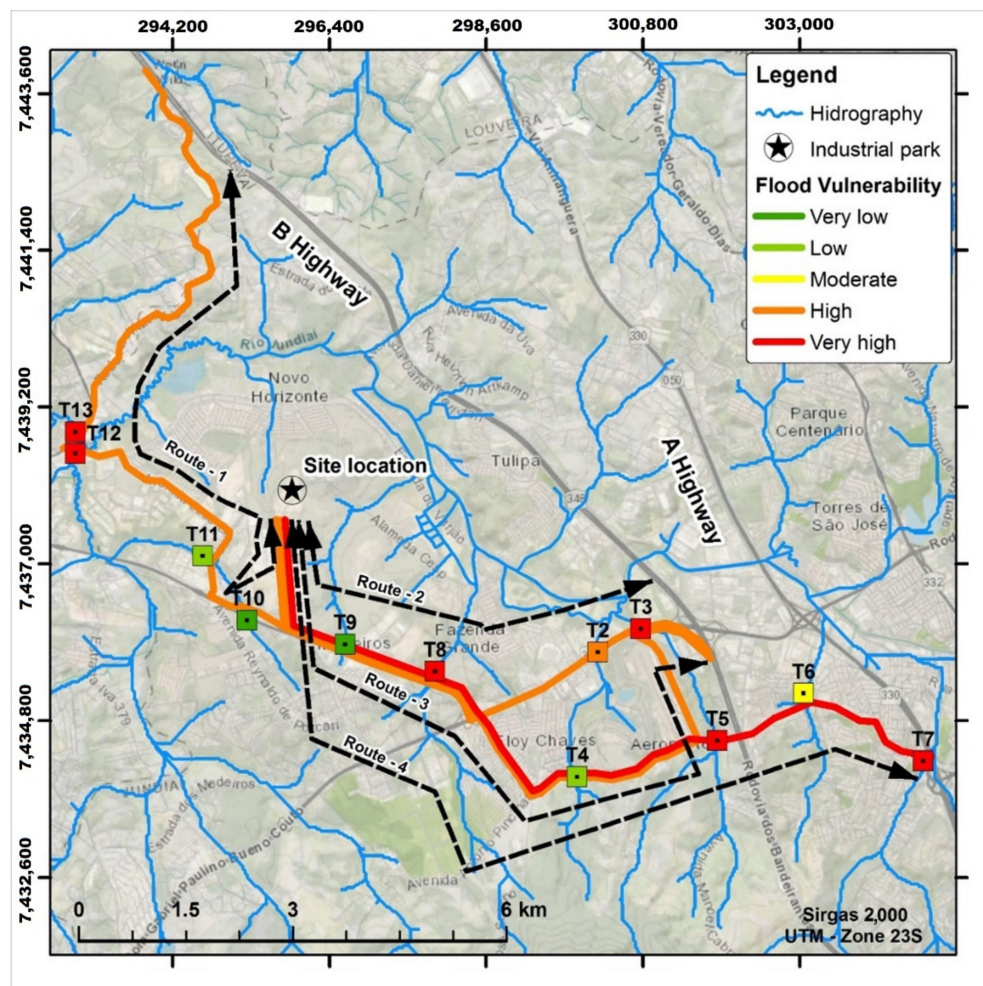

Figure 6. Flood vulnerability of potential routes to access the industrial park site.

The result shows that all four routes are vulnerable to floods; Route 1 is in a very high classification and all the others are in a high classification. It is important to emphasize that the result presented so far does not consider the flooding probability, analyzing only the propensity to suffer any damage from flood events.

4.3. Phase 3: The Flood Hazard Assessment
4.3.1. Characterization of the Watershed

The industrial park's watershed is pictured in Figure 7A. The topography information was obtained from the digital elevation model (DEM) of the Infrastructure and Environment Secretariat of the State of São Paulo (SIMA-SP), in the scale of 1:50,000 (GISAT project) and with a horizontal resolution of 30 m [30]. Physical information of the watershed can be found in Table 5.
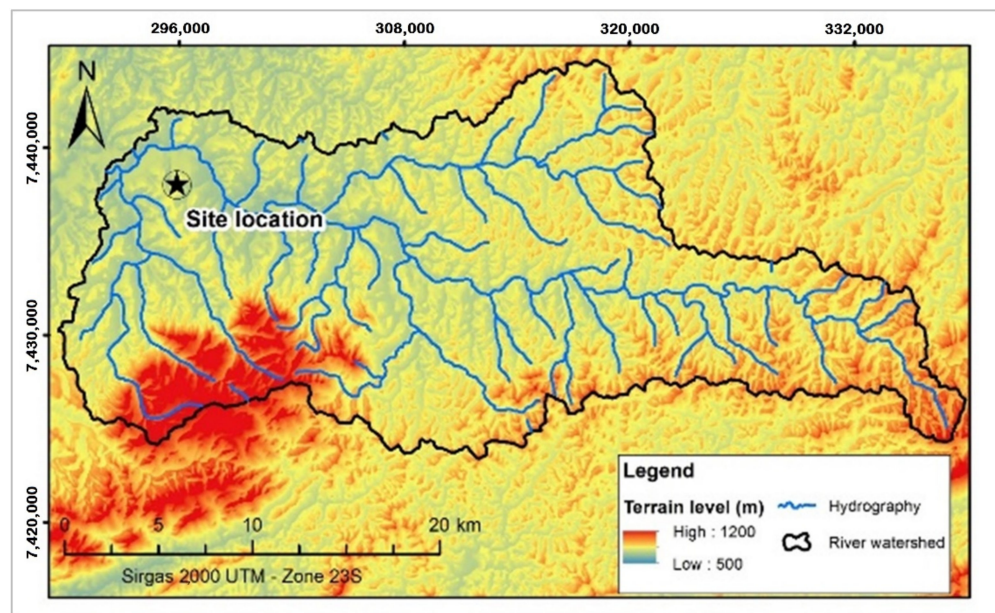
(**A**)
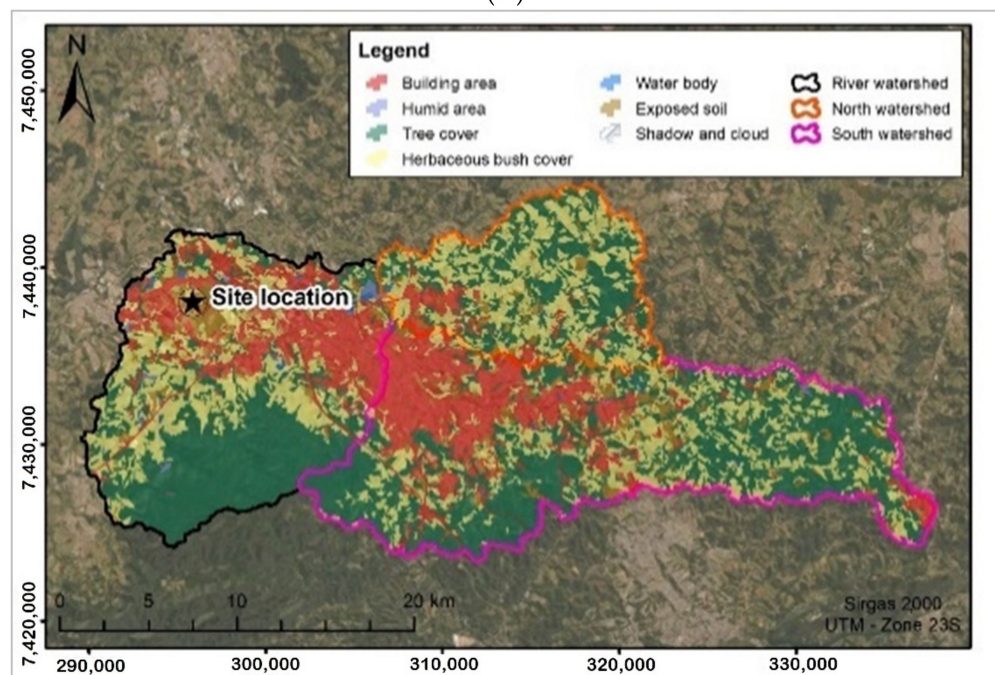
(**B**)

Figure 7. (**A**) Delimitation of the river watershed and (**B**) land use and land cover of the modeled area for industrial park site with the delimitation of the boundary conditions.

Table 5. Physical information of the river watershed–industrial park site.

Parameters	River Watershed
Drainage area	592.52 km^2
Maximum level difference	600 m
Length of the largest valley	61.36 km
Average slope	0.004726 m/m

Upstream areas were modeled using a hydrologic model, with the objective of estimating input hydrographs as boundary conditions to the hydrodynamic modeling domain. The hydrodynamic modeling domain covers different types of land use and cover, which

were analyzed to compose a weighted runoff coefficient, based on [55]. The final CN coefficient for the North and South watersheds is shown in Table 6.

Table 6. Land use and land cover for the composition of curve-number coefficient.

Land Use and Cover	North Watershed		South Watershed	
	Area	**CN**	**Area**	**CN**
Building area	9,973,249.35	77	63,760,635.71	77
Humid area	54,676.21	79	355,839.46	79
Tree cover	45,699,883.98	69	126,044,704.37	69
Herbaceous bush cover	49,738,638.28	60	65,108,219.38	60
Water body	373,536.74	100	542,563.55	100
Exposed soil	5,145,324.99	73	19,382,941.66	73
Final CN	66.6		67.6	

In Figure 7B, the two boundary conditions, the North and South watersheds, are represented, as well as the existing types of land use of the watershed.

4.3.2. Design Storm

The design rainfall was estimated through the intensity-duration-frequency relationship. The time of concentration was estimated through the equation of George Ribeiro [56], defined as follows (Equation (7)):

$$t_c = \frac{16.L}{(1.05 - 0.2p)(100.S)^{0.04}}$$ (7)

where:

L—Length of main watershed valley (km);
S—Average slope of the basin (M/m);
p—Coefficient of vegetation cover of the basin.

The time of concentration of the watershed taking the industrial park site as reference is estimated at 1114.14 min. To use a critical rainfall for the modeled area, a design rainfall of 1440 min, equivalent to the time of concentration of the watershed, was calculated, allowing for the evaluation of a critical flood peak.

From this rainfall duration, the intensity and precipitation height were calculated for the simulation scenario, using two rainfall equations (IDF) for two rain gauges. The first IDF was the equation from the DAEE (Department of Water and Electric Energy of São Paulo) [57] for the rain gauge 1, defined by:

$$i_{t,T} = 29.91 (t + 20)^{-0.862} + 21.61 (t + 30)^{-1.0438}[-0.4886 - 0.9212 \, lnln(T/T - 1)]$$ (8)

where:

i—rainfall intensity, corresponding to the duration t and recurrence time T, in mm/min;
T—recurrence time in years;
t—duration of rainfall in minutes.

The second one was the equation from *Observatório* IAG Station by [57], for rain gauge 2, defined by:

$$i_{t,T} = (t + 20)^{-0.9483} * 42.081 \, T^{0.1429}$$ (9)

where:

i—rainfall intensity, corresponding to the duration t and recurrence time T, in mm/min;
T—recurrence time in years;
t—duration of rainfall in minutes.

The Thiessen polygon method was used to define the influence areas of each considered gauge, as shown in Figure 8. Table 7 shows the total height for both rainfall design events in both rain gauges.
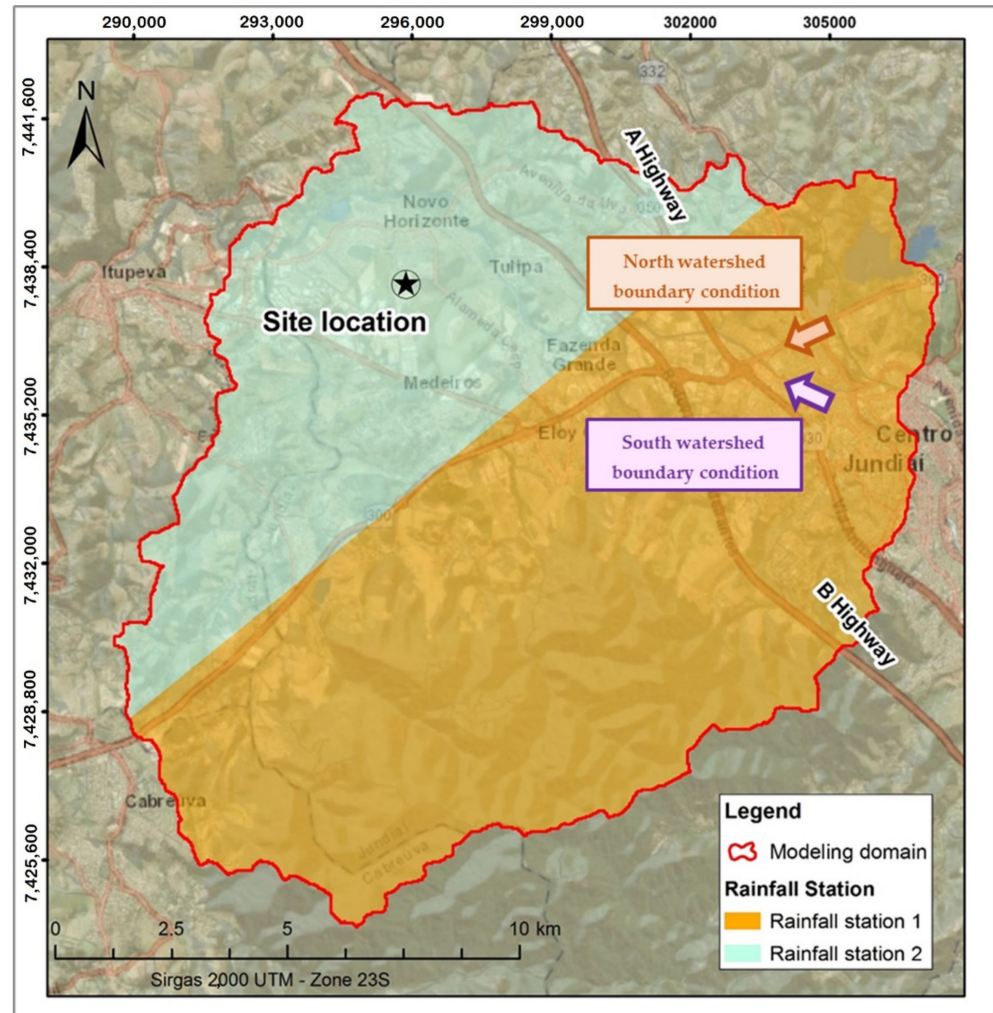
Figure 8. Areas of influence of the rainfall stations in the modeling domain of industrial park.

Table 7. Design storms for hydrological-hydrodynamic model.

	Rain Gauge 1		Rain Gauge 2	
Recurrence time	RP100 Years	RP500 Years	RP100 Years	RP500 Years
Total rainfall (mm)	138	161	117	147

The watersheds of the boundary conditions are entirely located within the area of influence of the rain gauge 1.

4.3.3. Hydrodynamic Studies

The modeled domain in the studied region is 216 km^2 and was discretized in a grid of 59,985 cells with 3600 m^2 each. The map of Figure 9 shows the runoff used in the hydrodynamic studies for the domain area where the industrial park lies. The manning and the runoff coefficient used for each land cover are presented in Table 8.
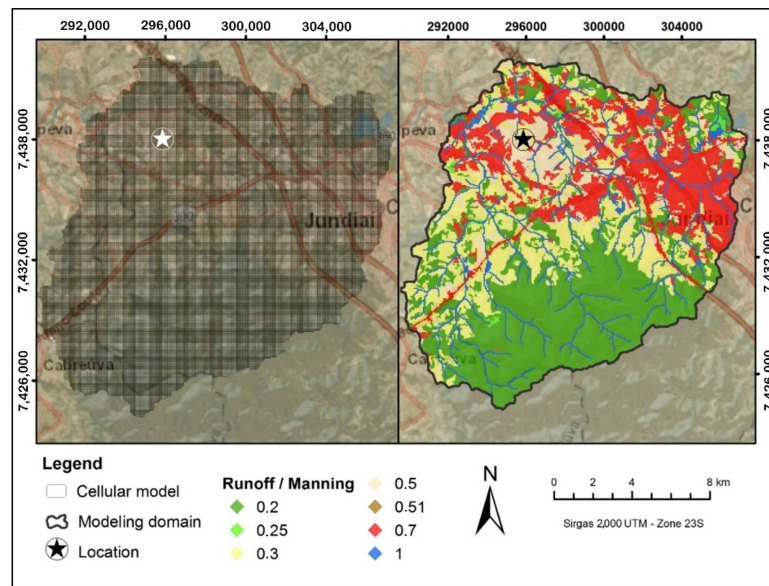
Figure 9. Model domain for industrial park and runoff coefficient for the model domain, representing the land cover of the area.

The simulation results of the flood depths for both events of RP100 years and RP500 years are presented in Figure 10.
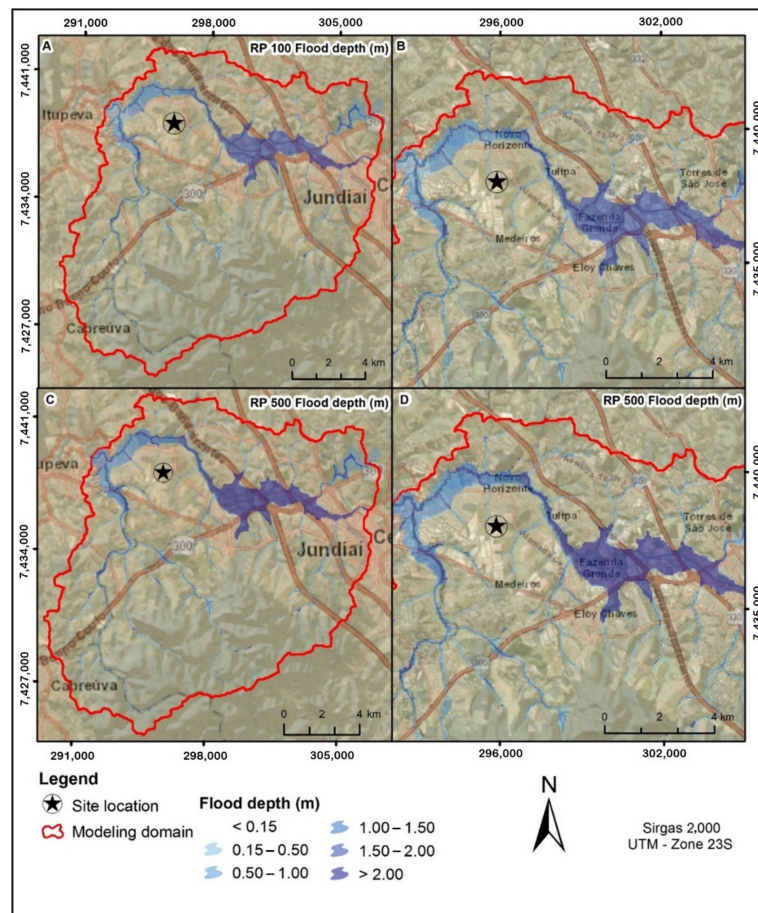
Figure 10. Flood depth results–industrial park. (**A**) Return period (RP) of 100 years design storm. (**B**) RP of 100 years design storm zoomed to industrial park region. (**C**) RP of 500 years design storm. (**D**) RP of 500 years design storm zoomed to industrial park region.

Table 8. Manning and runoff coefficients for the modeled area.

Land Cover	Manning Coefficient	Runoff Coefficient
Building area	0.100	0.80
Humid area	0.060	0.90
Tree cover	0.150	0.20
Herbaceous bush cover	0.080	0.35
Water body	0.033	1.00
Exposed soil	0.030	0.40
Shadow and cloud	0.031	0.60

Although the location of the industrial park has no direct contact with flooding waters, the region has a very critical situation. The main river valley localized close to the A and B highways suffers from severe flood depths.

Additionally, the flood discharges of rivers at bridges and culverts were evaluated to verify potential impacts on drainage structures. These points are shown in Figure 11
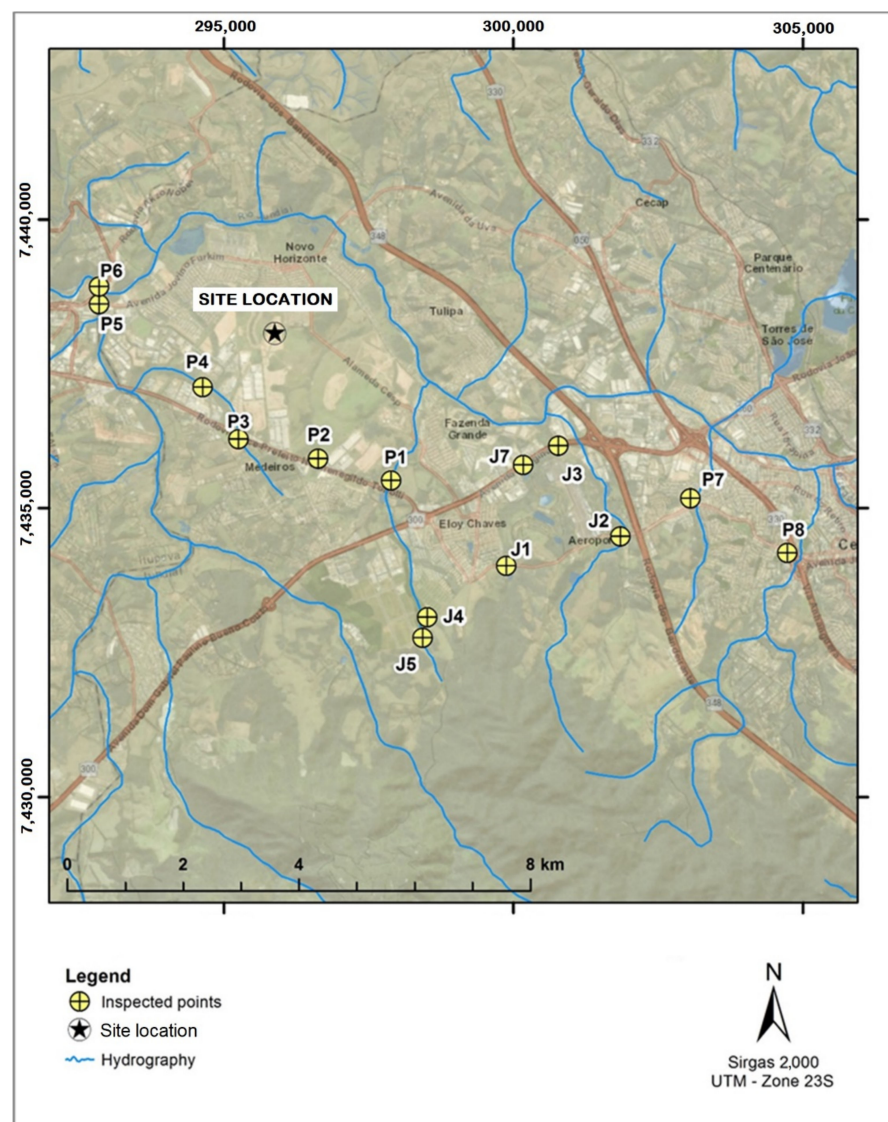

Figure 11. Localization of inspected points.

Table 9 shows the result of the hydraulic evaluation of river crossings in the industrial park region, highlighting the estimated flood discharges and hydraulic capacity of the drainage structures.

Table 9. Hydraulic evaluation of river crossings in industrial park region.

| | | Singularity | | | Estimated Discharge (m³/s) | | |
	Cross Section	Bottom Slope (m/m)	Adopted Manning	Hydraulic Capacity (m³/s)	RT100	RT500	Situation
J2	Culvert (3.0 m × 3.0 m)	0.0061	0.02	35.15	52.38	64.73	Overcapacity for both design discharges
J3	Double Culvert (3.0 m × 3.0 m)	0.0010	0.02	28.46	32.7	36.79	Overcapacity for both design discharges
J4	Culvert (2.7 m × 1.6 m)	0.0003	0.02	3.04	12.14	15.7	Overcapacity for both design discharges
J5	Culvert (2.0 m × 1.6 m)	0.0374	0.02	22.39	2.46	3.14	Adequate for both design discharges
J7	Culvert (3.0 m × 1.6 m)	0.0692	0.02	48.82	27.14	39.44	Adequate for both design discharges
P1				No visual access			
P2				No visual access			
P3	Culvert (D = 1.5 m)	0.0596	0.02	11.22	8.66	10.96	Adequate for both design discharges
P4	Culvert (D = 1.5 m)	0.0100	0.02	4.59	12.85	24.09	Overcapacity for both discharges
P5	Bridge (8.0 m × 4.0 m)	0.0050	0.035	102.63	57.87	73.37	Adequate for both design discharges
P6	Bridge (18.0 m × 8.0 m)	0.0050	0.035	761.56	40.53 *	43.82 *	Adequate for both design discharges
P7	Double Culvert (2.0 m × 2.0 m and D = 1.5 m)	0.0042	0.02	12.87	37.58	44.89	Overloaded for both discharges
P8	Double Culvert (3.0 m × 2.0 m)	0.0024	0.02	35.08	76.25	104.15	Overloaded for both discharges

* The simulated discharges in this point are underestimated, as a consequence of modeling aspects limitations. The scale of input data gives this bias to simulated flood discharges, but it does not affect the flood mapping. The evaluation of the flood peak must be carried out with more detailed data.

4.3.4. The Flood Hazard Assessment

The results of the flood hazard evaluation considering the storm with return periods of 100 years and 500 years are presented in Figure 12.

The areas with very high hazard classifications are concentrated along the valleys of rivers, showing two critical zones: between the A and B highways and in the basin outfall region. This last region presents a large and occupied area impacted by flooding that has high and very high hazard indicators.

As it was expected, the area closest to the industrial park site is not prone to a flood hazard, but the general situation of the watershed, within the modeling domain, shows large areas with high and very high hazard classification, that can affect the normal operation of transportation and public services.
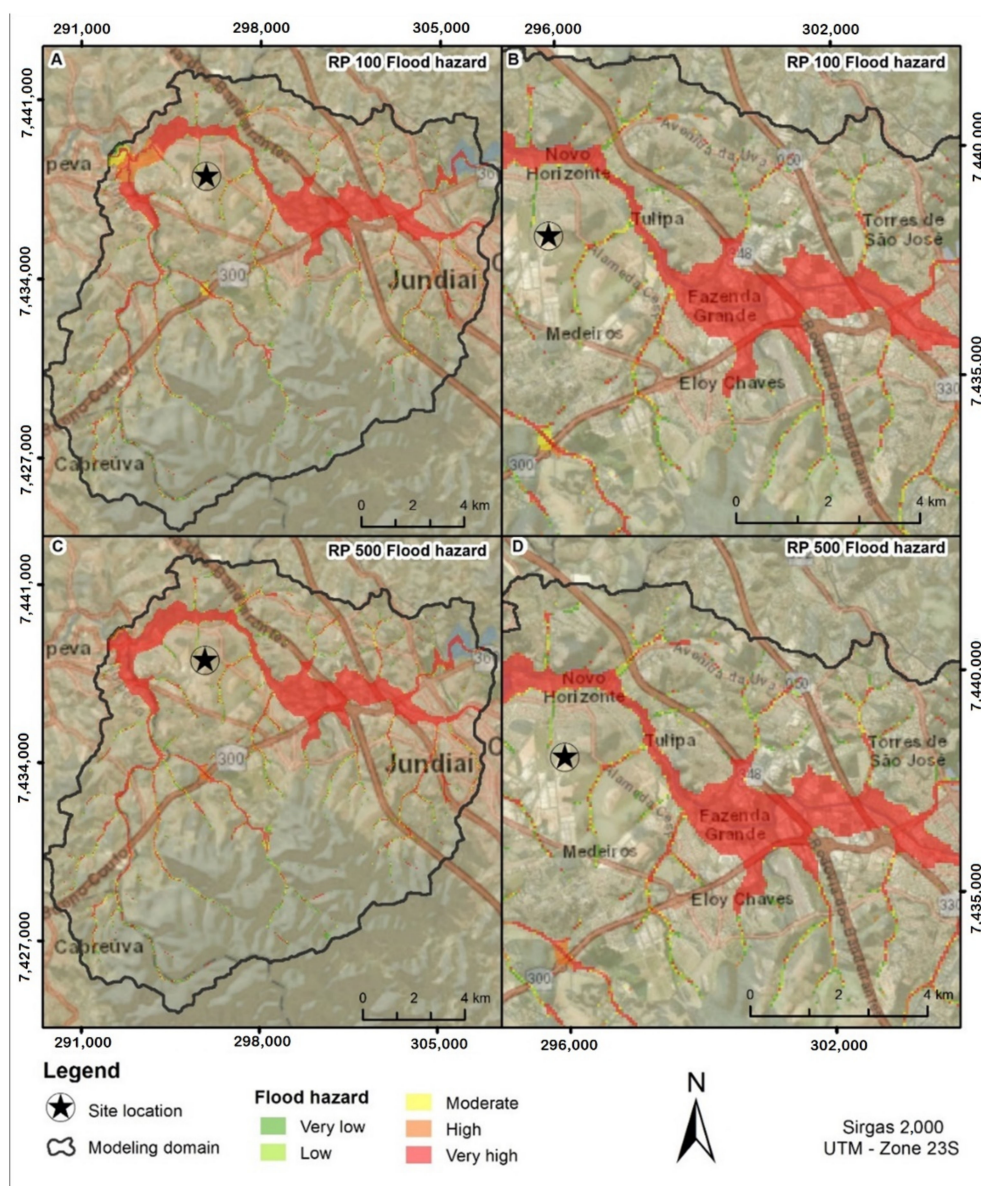
Figure 12. Mapping of flood hazard-industrial park. (**A**) 100 years' recurrence time storm. (**B**) 100 years' recurrence time storm zoomed to industrial park site. (**C**) 500 years' recurrence time storm. (**D**) 500 years' recurrence time storm zoomed to industrial park site.

4.4. Phase 4: The Risk Assessment

In the case of this study, the flood risk expresses the probability of an area to become flooded and cause difficulties in the access to the industrial park.

For the evaluation of the flood risk of the mobility system, the risk of each route was calculated considering the relation between the hazard indicators encountered along the route path and the route vulnerability (see the explanation in item "4.2. Phase 2: The Flood Vulnerability Assessment" and "4.3. Phase 3: The Flood Hazard Assessment").

The industrial park was classified as having a very high flood risk with a final average classification of 0.86 (in a scale from 0.00 to 1.00), as shown in Table 10.

Table 10. Flood risk assessment of Mobility System of industrial park site.

Route	Route Vulnerability	Route Hazard *	Route Risk	Site Flood Risk
Rt 1	1.00	0.94	0.95	
Rt 2	0.63	1.00	0.89	0.86
Rt 3	0.54	1.00	0.85	
Rt 4	0.70	0.68	0.75	

* Maximum moving average of three consecutive cells (~180 m) calculated by combining recurrence results 100 and 500 years.

5. Discussions and Conclusions

Floods, especially the ones resulting from intense precipitation, are the predominant cause of weather-related disruption of the transport sector. As the transportation network enables the movement of people and goods and is the basis of economic activity, its disruption may have drastic socio-economics consequences.

Since extreme weather events can cause direct or indirect damage to the transport sector, many researchers have developed methodologies for flood risk assessment, considering the transport system disruption. In most cases, when considering the impact of flooding on transport disruption, it is assumed that a road is either 'open' or 'closed'. However, flooding on a road does not necessarily preclude people from driving along it.

In this sense, the aim of this paper was to present a framework, based in hydrodynamic modeling, to establish a relationship between flood depths and the disruption of the road transport system. This new approach combines the vector information of the highway network that serves the region with the result of a quasi 2-D raster flood model, generating a set of interpreting rules for classifying the safety of routes.

The proposed methodology was used to assess the likelihood that a new industrial region, located in the state of São Paulo (Brazil), could be flooded, causing the disruption of the mobility system and local economic activities. It can be particularly interesting for decision-makers to plan alternative paths and strategies in advance to reduce flood-induced delays.

The proposed framework was elaborated in four phases. The first phase was the identification of previous studies that helped to better understand the region where the site is located, identify the most flood prone areas, and create the bases to assess flood vulnerability.

The second phase is the flood vulnerability assessment. Considering that the area is well above the quota of the valleys of the rivers nearby, the vulnerability and flood risk analysis was based on the possibility of the disruption of the mobility system. In this study, the vulnerability assessment considered the number of available alternative routes and the river crossings on their way. The results of the flood vulnerability assessment show that all four routes that connect the industrial park to the most important highways in the region are classified as high or very high, regarding flood vulnerability. This situation highlights the transport infrastructure vulnerability.

The third phase is the flood hazard assessment. In this study, the hazard analysis is based on the result of hydrological studies and hydrodynamic simulation of intense rainfall over the watershed. The floods resulting from hydrological events with 100 and 500 years of recurrence time were evaluated and the extent and depth of flooding in each event were determined. To understand these hydraulic phenomena in a more systemic way and to make more accurate estimates of their consequences, mathematical hydrodynamic models must be used. For the hydrodynamic studies, the modeling tool called MODCEL, a quasi-2D model [32], was used as a raster model to represent the region of interest.

The fourth and final phase is the risk analysis. The flood risk assessment is a combined evaluation of the vulnerability and hazard analyses that aims to determine the possible effects of flood events on the mobility system of the industrial park, indicating the dis-

ruption of its operation. The result of risk analysis showed that the mobility system is a critical item.

The proposed methodology is adherent with some recent research carried out by many authors, as it considered that there is a relationship between flood depth and a decrease in traffic velocity [15,20,24–27]. The obtained results indicate that the proposed methodology can achieve reliable and sound results.

However, it is noteworthy that this framework is highly dependent on physical and flood information during the elaboration and calibration of the model. These data, and especially the ones related to the river crossings main characteristics, are not easily found information. Despite this, the proposed framework proved to be satisfactory in evaluating the possible effects of flood events on the accessibility of the industrial park, indicating the possible disruption to economic activities and transportation, and allowing for planning alternatives in advance.

The results also showed that, to reduce the vulnerability of the industrial park, it is necessary to create alternative routes or to increase its flood defense. However, these mitigating measures may be infeasible, as they go beyond the private sphere, and are very costly. It is important to emphasize that characterizing the possible safe places to direct routes to is a step to be thought about calmly and confirmed with the existing and/or created flood spots.

Another relevant point is the computational performance and the modeling method adopted. It is observed that the size and detail of the area to be modeled can make modeling unfeasible. However, this modeling approach was capable of providing an equilibrium between the best resolution of the modelled area and the computational cost, allowing the creation of a relationship between the flood depths and the disruption of the road transport system.

Finally, it is important to notice that this framework was applied in a case study but can be replicated for similar problems of flood risks to mobility.

Author Contributions: Conceptualization, M.M.d.S. and M.G.M.; methodology, M.M.d.S. and O.M.R.; software, M.G.M.; modelling, M.M.d.S., O.M.R., A.C.P.J., G.M. and L.B.d.F.R.; formal analysis, M.M.d.S., O.M.R., A.C.P.J., G.M. and L.B.d.F.R.; writing, M.M.d.S. and P.M.C.d.M.; editing, M.M.d.S. and P.M.C.d.M.; review, M.G.M.; publishing, M.G.M. All authors have read and agreed to the published version of the manuscript.

Conflicts of Interest: The authors declare no conflict of interest.

References

1. Barendrecht, M.H.; Viglione, A.; Blöschl, G. A dynamic framework for flood risk. *Water Secur.* **2017**, *1*, 3–11. [CrossRef]
2. Rezende, O.M.; Miranda, F.M.; Haddad, A.N.; Miguez, M.G. A framework to evaluate urban flood resilience of design alternatives for flood defence considering future adverse scenarios. *Water* **2019**, *11*, 1485. [CrossRef]
3. Yazdani, M.; Mojtahedi, M.; Loosemore, M. Enhancing evacuation response to extreme weather disasters using public transportation systems: A novel simheuristic approach. *J. Comput. Des. Eng.* **2020**, *7*, 195–210. [CrossRef]
4. Miguez, M.G.; Veról, A.P. A catchment scale Integrated Flood Resilience Index to support decision making in urban flood control design. *Environ. Plan. B Urban Anal. City Sci.* **2017**, *44*, 925–946. [CrossRef]
5. FIESP. *XXII FIESP/CIESP Week—Environment*; Federação das Indústrias do Estado de São Paulo—FIESP: São Paulo, Brazil, 2010; Volume 1, pp. 1–44.
6. Kappes, M.S.; Keiler, M.; Elverfeldt, K. Von Challenges of analyzing multi-hazard risk: A review. *Nat. Hazards* **2012**, *64*, 1925–1958. [CrossRef]
7. Ward, P.J.; Blauhut, V.; Bloemendaal, N.; Daniell, J.E.; de Ruiter, M.C.; Duncan, M.J.; Emberson, R.; Jenkins, S.F.; Kirschbaum, D.; Kunz, M.; et al. Review article: Natural hazard risk assessments at the global scale. *Nat. Hazards* **2020**, *20*, 1069–1096. [CrossRef]

8. UNISDR. *Terminology on Disaster Risk Reduction*; United Nations International k Reduction Strategy for Disaster Reduction (UNISDR): Geneva, Switzerland, 2009.

9. Plate, E.J. Flood risk and flood management. *J. Hydrol.* **2002**, *267*, 2–11. [CrossRef]

10. Antwi, E.K.; Boakye-Danquah, J.; Barima Owusu, A.; Loh, S.K.; Mensah, R.; Boafo, Y.A.; Apronti, P.T. Community vulnerability assessment index for flood prone savannah agro-ecological zone: A case study of Wa West District, Ghana. *Weather Clim. Extrem.* **2015**, *10*, 56–69. [CrossRef]

11. Souza, C.R.G. Risco a inundações, enchentes e alagamentos em regiões costeiras. In Proceedings of the Simpósio Brasileiro de Desastres Naturais GEDN/UFSC, Florianópolis, Brazil, 27–30 September 2004; pp. 231–247.

12. Tingsanchali, T. Urban flood disaster management. *Procedia Eng.* **2012**, *32*, 25–37. [CrossRef]

13. Bennet, B.T. *Understanding, Assessing, and Responding to Terrorism: Protecting Critical Infrastructure and Personnel*; Wiley & Sons: New York, NY, USA, 2018.

14. Rinaldi, S.M.; Peerenboom, J.P.; Kelly, T.K. Identifying, understanding, and analyzing critical infrastructure interdependencies. *IEEE Control Syst.* **2001**, *21*, 11–25. [CrossRef]

15. Najafi, M.R.; Zhang, Y.; Martyn, N. A flood risk assessment framework for interdependent infrastructure systems in coastal environments. *Sustain. Cities Soc.* **2021**, *64*, 102516. [CrossRef]

16. Yang, Y.; Ng, S.T.; Xu, F.J.; Skitmore, M. Towards sustainable and resilient high density cities through better integration of infrastructure networks. *Sustain. Cities Soc.* **2018**, *42*, 407–422. [CrossRef]

17. Hammond, M.J.; Chen, A.S.; Djordjevic, S.; Butler, D.; Mark, O. Urban flood impact assessment: A state-of-the-art review. *Urban Water J.* **2015**, *12*, 14–29. [CrossRef]

18. Qiang, Y. Flood exposure of critical infrastructure in the United States. *Int. J. Disaster Risk Reduct.* **2019**, *39*, 101240. [CrossRef]

19. Vamvakeridou-Lyroudia, L.S.; Chen, A.S.; Khoury, M.; Gibson, M.J.; Kostaridis, A.; Stewart, D. Assessing and visualising hazard impacts to enhance the resilience of Critical Infrastructure to urban flooding. *Sci. Total Environ.* **2020**, *707*, 136078. [CrossRef]

20. Pregnolato, M.; Ford, A.; Wilkinson, S.M.; Dawson, R.J. The impact of flooding on road transport: A depth-disruption function. *Transp. Res. Part D Transp. Environ.* **2017**, *55*, 67–81. [CrossRef]

21. Argyroudis, S.A.; Mitoulis, S.; Winter, M.G.; Kaynia, A.M. Fragility of transport assets exposed to multiple hazards: State-of-the-art review toward infrastructural resilience. *Reliab. Eng. Syst. Saf.* **2019**, *191*, 106567. [CrossRef]

22. Rozenberg, J.; Alegre, X.E.; Avner, P.; Fox, C.; Koks, S.H.E.; Tariverdi, J.R.M. From a Rocky Road to Smooth Sailing. In Proceedings of the Irish Economic Association Annual Conference 2017, Dublin, Ireland, 4–5 May 2017.

23. Zhang, N.; Alipour, A. A multi-step assessment framework for optimization of flood mitigation strategies in transportation networks. *Int. J. Disaster Risk Reduct.* **2021**, *63*, 102439. [CrossRef]

24. Fereshtehpour, M.; Burian, S.J.; Karamouz, M. Flood Risk Assessments of Transportation Networks Utilizing Depth-Disruption Function. *World Environ. Water Resour. Congr.* **2018**, *1*, 134–142. [CrossRef]

25. Choo, K.-S.; Kang, D.-H.; Kim, B.-S. Impact Assessment of Urban Flood on Traffic Disruption using Rainfall—Depth—Vehicle speed relationship. *Water* **2020**, *12*, 926. [CrossRef]

26. Abdulla, B.; Kiaghadi, A.; Rifai, H.S.; Birgisson, B. Characterization of vulnerability of road networks to fluvial flooding using SIS network diffusion model. *J. Infrastruct. Preserv. Resil.* **2020**, *1*, 6. [CrossRef]

27. Singh, P.; Sinha, V.S.P.; Vijhani, A.; Pahuja, N. Vulnerability assessment of urban road network from urban flood. *Int. J. Disaster Risk Reduct.* **2018**, *28*, 237–250. [CrossRef]

28. Sohn, J. Evaluating the significance of highway network links under the flood damage: An accessibility approach. *Transp. Res. Part A* **2006**, *40*, 491–506. [CrossRef]

29. *Fehidro Plano Estadual de Recursos Hídricos 2020–2023—Resumo Executivo*; Government of São Paulo: São Paulo, Brazil, 2020.

30. SMA Modelo Digital de Elevação (MDE) do Estado de São Paulo. Available online: https://www.infraestruturameioambiente.sp. gov.br/cpla/modelo-digital-de-elevacao-mde-do-estado-de-sao-paulo/ (accessed on 3 September 2021).

31. James, W.P.; Winsor, P.W.; Williams, J.R. Synthetic Unit Hydrograph. *J. Water Resour. Plan. Manag.* **1987**, *113*, 70–81. [CrossRef]

32. Mascarenhas, F.C.B.; Miguez, M.G. Urban Flood Control through a Mathematical Cell. *Water Int.* **2002**, *27*, 208–218. [CrossRef]

33. Zanobetti, D.; Lorgeré, H. Le modèle mathématique du delta du mékong. *La Houille Blanche* **1968**, *5*, 363–378. [CrossRef]

34. Cunge, J.A.; Holly, F.M., Jr.; Verwey, A. *Practical Aspects of Computational River Hydraulics*; Pitman Advanced Publishing Program Ed.; The Pitman Press: London, UK, 1980.

35. Miguez, M.G.; Battemarco, B.P.; de Sousa, M.M.; Rezende, O.M.; Veról, A.P.; Gusmaroli, G. Urban flood simulation using MODCEL-an alternative quasi-2D conceptual model. *Water* **2017**, *9*, 445. [CrossRef]

36. Jacob, A.C.P.; Rezende, O.M.; de Sousa, M.M.; de França Ribeiro, L.B.; de Oliveira, A.K.B.; Arrais, C.M.; Miguez, M.G. Use of detention basin for flood mitigation and urban requalification in Mesquita, Brazil. *Water Sci. Technol.* **2019**, *79*, 10. [CrossRef]

37. Moura Rezende, O.; Ribeiro da Cruz de Franco, A.B.; Beleño de Oliveira, A.K.; Pitzer Jacob, A.C.; Gomes Miguez, M. A framework to introduce urban flood resilience into the design of flood control alternatives. *J. Hydrol.* **2019**, *576*, 478–493. [CrossRef]

38. Scionti, F.; Miguez, M.G.; Barbaro, G.; de Sousa, M.M.; Foti, G.; Canale, C. Integrated Methodology for Urban Flood Risk Mitigation in Cittanova, Italy. *J. Water Resour. Plan. Manag.* **2018**, *144*, 05018013. [CrossRef]

39. Nardini, A.; Gomes Miguez, M. An Integrated Plan to Sustainably Enable the City of Riohacha (Colombia) to Cope with Increasing Urban Flooding, while Improving Its Environmental Setting. *Sustainability* **2016**, *8*, 198. [CrossRef]

40. Miguez, M.G.; Veról, A.P.; de Sousa, M.M.; Rezende, O.M. Urban floods in lowlands-levee systems, unplanned urban growth and river restoration alternative: A case study in Brazil. *Sustainability* **2015**, *7*, 11068–11097. [CrossRef]
41. Bates, P.D.; Horritt, M.S.; Fewtrell, T.J. A simple inertial formulation of the shallow water equations for efficient two-dimensional flood inundation modelling. *J. Hydrol.* **2010**, *387*, 33–45. [CrossRef]
42. Castellarin, A.; Domeneghetti, A.; Brath, A. Identifying robust large-scale flood risk mitigation strategies: A quasi-2D hydraulic model as a tool for the Po river. *Phys. Chem. Earth* **2011**, *36*, 299–308. [CrossRef]
43. Dimitriadis, P.; Tegos, A.; Oikonomou, A.; Pagana, V.; Koukouvinos, A.; Mamassis, N.; Koutsoyiannis, D.; Efstratiadis, A. Comparative evaluation of 1D and quasi-2D hydraulic models based on benchmark and real-world applications for uncertainty assessment in flood mapping. *J. Hydrol.* **2016**, *534*, 478–492. [CrossRef]
44. Gregoretti, C.; Degetto, M.; Boreggio, M. GIS-based cell model for simulating debris flow runout on a fan. *J. Hydrol.* **2016**, *534*, 326–340. [CrossRef]
45. Horritt, M.S.; Bates, P.D. Predicting floodplain inundation: Raster-based modelling versus the finite-element approach. *Hydrol. Process.* **2001**, *15*, 825–842. [CrossRef]
46. Hunter, N.M.; Horritt, M.S.; Bates, P.D.; Wilson, M.D.; Werner, M.G.F. An adaptive time step solution for raster-based storage cell modelling of floodplain inundation. *Adv. Water Resour.* **2005**, *28*, 975–991. [CrossRef]
47. Moussa, R.; Bocquillon, C. On the use of the diffusive wave for modelling extreme flood events with overbank flow in the floodplain. *J. Hydrol.* **2009**, *374*, 116–135. [CrossRef]
48. Oikonomou, A.; Dimitriadis, P.; Koukouvinos, A.; Tegos, A.; Pagana, V.; Panagopoulos, P.; Mamassis, N.; Koutsoyiannis, D. Floodplain mapping via 1D and quasi-2D numerical models in the valley of Thessaly, Greece. In Proceedings of the European Geosciences Union General Assembly 2013, Vienna, Austria, 7–13 April 2013; Volume 15, p. 10366.
49. Paz, A.R.; Collischonn, W. River reach length and slope estimates for large-scale hydrological models based on a relatively high-resolution digital elevation model. *J. Hydrol.* **2007**, *343*, 127–139. [CrossRef]
50. Skinner, C.J.; Coulthard, T.J.; Parsons, D.R.; Ramirez, J.A.; Mullen, L.; Manson, S. Simulating tidal and storm surge hydraulics with a simple 2D inertia based model, in the Humber Estuary, U.K. *Estuar. Coast. Shelf Sci.* **2015**, *155*, 126–136. [CrossRef]
51. Paz, A.R.D.; Collischonn, W.; Tucci, C.E.; Padovani, C.R. Large-scale modelling of channel flow and floodplain inundation dynamics and its application to the Pantanal (Brazil). *Hydrol. Process.* **2011**, *25*, 1498–1516. [CrossRef]
52. Horritt, M.S.; Bates, P.D. Evaluation of 1D and 2D numerical models for predicting river flood inundation. *J. Hydrol.* **2002**, *268*, 87–99. [CrossRef]
53. ANA. *Atlas de Vulnerabilidade a Inundações*; Agência Nacional de Águas (ANA): Brasilia, Brazil, 2014; p. 15.
54. CPRM. *Cartas de Suscetibilidade a Movimentos Gravitacionais de Massa e Inundações: 1:25.000 (Livro Eletrônico)*; CPRM: Brasilia, Brazil, 2014.
55. Wilken, P.S. *Engenharia de Drenagem Superficial (Superficial Drainage Engineering)*; CETESB: São Paulo, Brazil, 1978.
56. Ribeiro, G. Acerca do calculo da vasão de obras d'arte: Tempo de concentração. *Rev. Clube Eng.* **1961**, *294*, 16–19.
57. DAEE. *Equações de Chuvas Intensas do Estado de São Paulo*; Departamento de Águas e Energia Elétrica Ed.; Convênio Departamento de Águas e Energia Elétrica e Escola Politécnica da Universidade de São Paulo: São Paulo, Brazil, 1999.